

‘Gas cushion’ model and hydrodynamic boundary conditions for superhydrophobic textures.

Tatiana V. Nizkaya,¹ Evgeny S. Asmolov,^{1,2,3} and Olga I. Vinogradova^{1,4,5,*}

¹*A.N. Frumkin Institute of Physical Chemistry and Electrochemistry,*

Russian Academy of Sciences, 31 Leninsky Prospect, 119071 Moscow, Russia

²*Central Aero-Hydrodynamic Institute, 140180 Zhukovsky, Moscow region, Russia*

³*Institute of Mechanics, M. V. Lomonosov Moscow State University, 119991 Moscow, Russia*

⁴*Department of Physics, M. V. Lomonosov Moscow State University, 119991 Moscow, Russia*

⁵*DWI - Leibniz Institute for Interactive Materials,*

RWTH Aachen, Forckenbeckstraße 50, 52056 Aachen, Germany

Superhydrophobic Cassie textures with trapped gas bubbles reduce drag, by generating large effective slip, which is important for a variety of applications that involve a manipulation of liquids at the small scale. Here we discuss how the dissipation in the gas phase of textures modifies their friction properties. We propose an operator method, which allows us the mapping of the flow in the gas subphase to a local slip boundary condition at the liquid/gas interface. The determined uniquely local slip length depends on the viscosity contrast and underlying topography, and can be immediately used to evaluate an effective slip of the texture. Besides superlubricating Cassie surfaces our approach is valid for rough surfaces impregnated by a low-viscosity ‘lubricant’, and even for Wenzel textures, where a liquid follows the surface relief. These results provide a framework for the rational design of textured surfaces for numerous applications.

PACS numbers: 83.50.Rp, 47.61.-k, 68.03.-g

I. INTRODUCTION.

Superhydrophobic (SH) textures have raised a considerable interest and motivated numerous studies during the past decade. Such surfaces in the Cassie state, i.e., where the texture is filled with gas, can induce exceptional wetting properties [1] and, due to their superlubricating potential [2–5], are also extremely important in context of fluid dynamics. To quantify the drag reduction associated with two-component (e.g., gas and solid) SH surfaces with given area fractions it is convenient to construct the effective slip boundary condition (on the scale larger than the pattern characteristic length) for the averaged velocity field. This condition is applied at the imaginary smooth homogeneous surface [6, 7], which mimics the actual one and fully characterizes the flow at the real surface and is generally a tensor [8, 9]. Once eigenvalues of the slip-length tensor, which depend on both the hydrodynamic boundary condition at the solid/liquid interface and viscous dissipation in the gas phase, are determined, they can be used to solve complex hydrodynamic problems without tedious calculations. A key difficulty is that there is no general analytical theory that relates this dissipation to the relief of the texture, so that prior work often neglected it, by imposing idealized shear-free boundary conditions at the gas sectors [10–12].

To account for a dissipation within the gas subphase it is necessary to solve Stokes equations by applying condi-

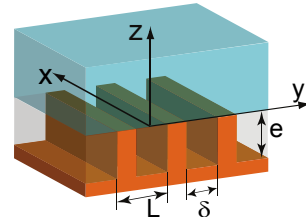


FIG. 1: Sketch of the typical 1D SH surface represented by rectangular grooves rigorously studied here, but some of our conclusions are general and apply for any 1D and 2D textured surfaces - pillars, holes, lamellae.

tions

$$z = 0 : \mathbf{u} = \mathbf{u}_g, \mu \frac{\partial \mathbf{u}_\tau}{\partial z} = \mu_g \frac{\partial \mathbf{u}_{g\tau}}{\partial z}, \quad (1)$$

where \mathbf{u} and μ are the velocity and the dynamic viscosity of the liquid, and \mathbf{u}_g and μ_g are those of the gas, $\mathbf{u}_\tau = (u_x, u_y)$ is the tangential velocity. Although this problem has been resolved numerically for rectangular grooves [13, 14], such a strategy appears rather hopeless in context of exact analytical results, especially for complex configurations, which are typical for many applications. An elegant semi-analytical approach based on an assumption of a constant shear inside the groove has been proposed recently [15]. Note that although this derivation made a significant step forward, it remains approximate and does not take into account the total dissipation in the gas subphase.

To bypass this problem, it is advantageous to replace the two-phase approach, by a single-phase problem with spatially dependent partial slip boundary condition [2,

*Corresponding author: oivinograd@yahoo.com

16], which takes a form

$$z = 0 : \mathbf{u}_\tau - b(x, y) \frac{\partial \mathbf{u}_\tau}{\partial z} = 0, \quad (2)$$

where $b(x, y)$ is the *local* slip length at the gas areas, which is normally assumed to conform the texture relief according to predictions of the ‘gas cushion’ model [17]

$$b^{x,y}(x, y) \simeq k^{x,y} \frac{\mu}{\mu_g} e(x, y), \quad (3)$$

where prefactors $k^{x,y} = 1$ can reduce to 1/4 if the net gas flux becomes zero (due to end walls) [18]. Such an approach, justified for a continuous gas layer at a homogeneous surface [17] and later for shallow grooves [18], is by no means obvious for an arbitrary texture, where the gas subphase can be deep and strongly confined. In such a situation it remains largely unknown if the gas flow can be indeed excluded from the analysis being equivalently replaced by $b(x, y)$, and how (and whether) this local slip profile is uniquely related to the relief of the texture.

In this article, we propose a general theoretical method, which allows us to generalize the ‘gas cushion’ model for any 1D and 2D two-phase SH textures in the Cassie state, or rough surfaces impregnated by a low-viscosity ‘lubricant’. We also show that our approach can be applied even for textures in the one-phase Wenzel state, where the liquid follows the topological variations of the texture.

II. THEORY.

A. General consideration

To illustrate our approach, we consider 1D SH surface of period L , and assume the interface to be flat with no meniscus curvature (see Fig. 1). Such an idealized situation, which neglects an additional mechanism for a dissipation due to a meniscus [19, 20], has been considered in most previous publications [6, 11, 21] and observed in recent experiments [22]. We then impose no-slip at the solid area, i.e. neglect slippage of liquid [23–26] and gas [27] past hydrophobic surface, which is justified provided the nanometric slip is small compared to parameters of the texture. No further assumptions are made, aside from distinguishing between longitudinal and transverse gas flow, with $k^x = 1$ and $k^y = 1/4$, to address the most anisotropic case.

The linearity of Stokes equations implies that the boundary condition at the liquid/gas interface for longitudinal and transverse directions can be formulated as:

$$z = 0 : \frac{\partial \mathbf{u}_{g\tau}}{\partial z} - \mathbf{P}^{x,y}[\mathbf{u}_{g\tau}] = 0, \quad (4)$$

where we introduced the linear operator $\mathbf{P}^{x,y}$ that belongs to a general class of Dirichlet-to-Neumann (DtN) ones [28]. The meaning of Eq.(4) becomes clear if we

project both the velocity and its normal derivative on a grid $\{y_i\}_{i=1}^N$ at the liquid/gas interface. Then the operator becomes a matrix P_{ij} that relates the shear rate at a given point i with velocities in every other points of the interface $j = 1..N$ (the condition is essentially *nonlocal*). Unlike the local slip length, the operator depends only on the texture relief, but not on the solution outside. It is universal and, once calculated for a given topography, can be applied for any geometry of the outside flow and any viscosity ratio. Then, in view of Eq.(1), the non-local boundary condition for fluid flow past a SH surface reads:

$$\frac{\partial u_{x,y}(y_i, 0)}{\partial z} - \frac{\mu}{\mu_g} \sum_{j=1}^N P_{ij}^{x,y} u_{x,y}(y_j, 0) = 0, \quad i = 1..N. \quad (5)$$

This boundary condition allows to solve the Stokes equations for the liquid phase separately and to determine the local slip length by using Eq.(2):

$$b^{x,y}(y) = \frac{\mu}{\mu_g} \frac{u_{x,y}(y, 0)}{\mathbf{P}^{x,y}[u_{x,y}]}. \quad (6)$$

We recall that the local slip length may depend not only on the texture relief, but also on the state of the liquid phase, which could affect the velocity $u_{x,y}$. However, for a single surface we consider here the local slip length is uniquely related to the texture relief and the generalization of the ‘gas cushion’ model can be constructed. For confined configurations (e.g. flow in a thin channel) the local slip length will of course be a property of the whole system, but note that the $\mathbf{P}^{x,y}$ -operators will remain exactly the same.

To calculate the matrices $P_{ij}^{x,y}$ we should solve the problem in the gas phase and extract the normal derivative of the solution either analytically or numerically. In this paper we rigorously calculate them for a rectangular groove using a Fourier method. For an arbitrary 1D geometry $\mathbf{P}^{x,y}$ can be expressed in the form of a boundary integral operator involving Green’s functions for the Stokes flow [29]. As a side note, we remark that it can be similarly constructed for 2D surfaces, but of course by using Green’s functions for 3D Stokes flow [29]. Note however that one does not expect the main physical picture to be altered in these (more technically challenging) situations, and we leave the study of these complex geometries for a future work.

B. Periodic rectangular grooves.

For an initial application of our approach, we consider now periodic rectangular grooves of width δ and depth e . The fraction of gas area is then $\phi = \delta/L$. In this particular case the problem inside the groove can be solved using the Fourier method. For the longitudinal flow this yields an analytical expression for the DtN matrix:

$$P_{ij}^x = \frac{1}{\delta} \left(F_{im} \Pi_{ml} F_{lj}^{-1} \right), \quad (7)$$

$$F_{im} = \cos(k_m^* y_i / \delta), \quad \Pi_{ml} = k_m^* \coth(k_m^* e / \delta) \delta_{ml},$$

where $k_m^* = (2m - 1)\pi$ and δ_{ml} is the Kronecker delta. Note that the matrix combination inside the brackets in Eq.(7) depends only on the aspect ratio, e/δ (and the spatial grid used). The same is true for the transverse direction, although the matrix P_{ij}^y can be obtained only semi-analytically (see Appendix B).

Having calculated $P_{ij}^{x,y}$, we can then use the Fourier method to solve the Stokes equations for liquid with the non-local boundary condition Eq.(5) (see Appendix A for details). We stress again that the resulting problem is not affected by the texture relief or the method used to find $P_{ij}^{x,y}$ due to a half-space liquid domain. From the liquid velocity field we can extract both the local slip length profile $b_{x,y}(y)$ (by using Eq. 6) and the effective slip tensor $b_{\text{eff}}^{\parallel,\perp}$ (by averaging over texture period) as will be discussed below.

III. RESULTS AND DISCUSSION.

A. Local slip length

Figs. 2(a) and (b) show profiles of the longitudinal, $b^x(y)$, and transverse, $b^y(y)$, local slip lengths at fixed groove width, $\delta/L = 0.75$, and aspect ratio, e/δ , varying from 0.1 to infinity. The calculations are made using $\mu/\mu_g = 50$, which corresponds to a SH texture filled with gas. It can be seen that for shallow grooves, $e/\delta \ll 1$, local slip lengths saturate to constant values predicted by Eq.(3) at the central part of the gas sector, but $b^{x,y}(y)$ vanish at the edge of the groove. Thus the local slip profiles can be roughly approximated by a trapezoid [30].

For deeper grooves the local slip curves look more as parabolic. At $e/\delta \geq 1$ they converge to a single curve suggesting that $b^{x,y}(y)$ of deep grooves are controlled by the value of δ only, being independent on a texture depth. This result does not support Eq.(3), which predicts that $b^{x,y}(y)$ are growing infinitely with e , and indicates that for large e the dissipation at the edge of the grooves becomes crucial.

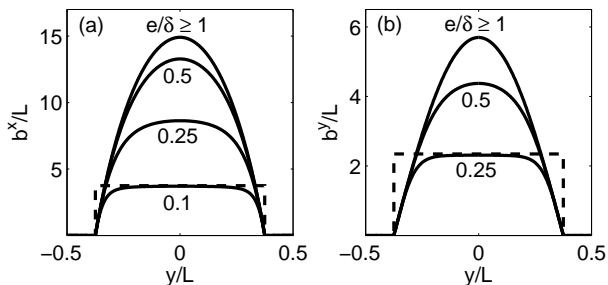


FIG. 2: Longitudinal (a) and transverse (b) local slip lengths computed with $\phi = 0.75$, $\mu/\mu_g = 50$. Dashed lines show the predictions of Eq.(3).

Indeed, the data presented in Figs. 2(a) and (b) suggest that near the edge of the groove $b^{x,y}$ always augment from

zero by having the same slope (which has not been taken into account in recent work [15]). This slope can be found by asymptotic analysis in the vicinity of the groove's edge. Motivated by an earlier single-phase analysis [31, 32], we can now construct the asymptotic solution for the two-phase flow near the edge by using polar coordinates (r, θ) (see Fig. 3(a) and Appendix C for details).

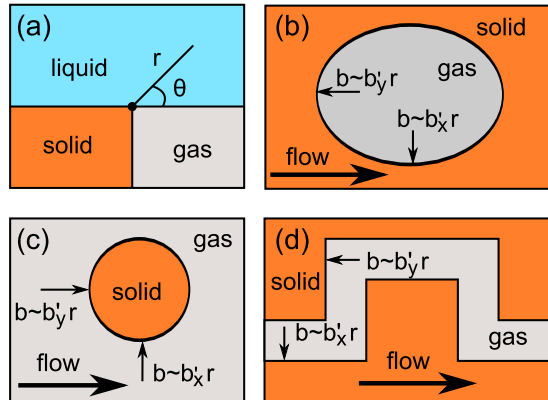


FIG. 3: Polar coordinates (side view) used to evaluate the flow near the edge of the groove, (a) and illustration (top view) of the local slip length behavior at the edge of 2D pillars (b), hollows (c) and channels (d).

Close to the edge, when $r \ll 1$, the general solution of the Stokes equations implies a power-law dependence of velocities on the distance, $u \propto r^\lambda$: $u_x = r^\lambda a \sin(\lambda\theta)$, $u_{gx} = r^\lambda [c \sin(\lambda\theta) + h \cos(\lambda\theta)]$. Similar arguments are valid for the transverse configuration. This yields a linear dependence for the slip lengths, $b^{x,y} = r \delta b'_{x,y}(\lambda)$. The exponent λ can be found from the boundary conditions at the solid walls and the liquid/gas interface.

For large μ/μ_g we obtain (see Appendix C):

$$b'_x \simeq 2\mu/\mu_g, \quad b'_y \simeq \mu/(2\mu_g). \quad (8)$$

The above expressions for b'_x and b'_y give upper and lower bounds on slopes among all textures, which are attained when the main flow is tangent or normal to the border of the gas area. Therefore, b^x is constrained by $\delta\mu/\mu_g$, and b^y by $\delta\mu/4\mu_g$ (see Fig.3(b-d)), so that the local slip profiles for arbitrary textures should be similar to shown in Fig.2, although the absolute value of maximum might differ.

It is natural now to propose a generalization of Eq.(3) for a SH surface, where we scale with δ instead of L :

$$b^{x,y}(y) = \delta \frac{\mu}{\mu_g} \beta^{x,y}(e/\delta, y/\delta). \quad (9)$$

Here we ascribe rescaled dimensionless local slip lengths, $\beta^{x,y}$, which become linear in e/δ when e/δ is small, and we recover Eq.(3). At the other extreme, when e/δ is large, $\beta^{x,y}$ saturate to provide an upper limit for local slip lengths.

To verify this Ansatz in Fig. 2 (a) and (b) we plot $\beta^{x,y}$ as a function of y/δ at different ϕ and e/δ . Here we use a

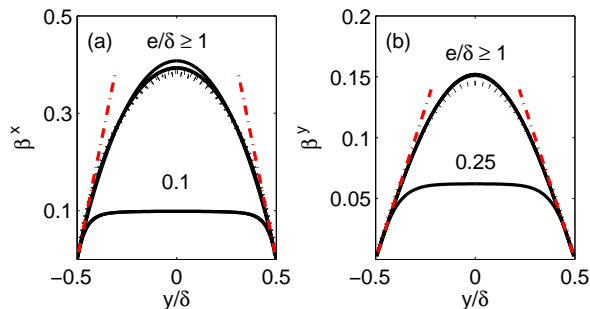


FIG. 4: Rescaled longitudinal (a) and transverse (b) local slip-length for deep and shallow grooves. Solid and dotted curves correspond to the Cassie, $\mu/\mu_g = 50$, and Wenzel, $\mu/\mu_g = 1$, states at $\phi = 0.1, 0.5, 0.9$ (these curves coincide for shallow grooves and are nearly overlapping for deep grooves). Dash-dotted lines show asymptotic solutions near the edges of the groove.

viscosity ratio of the Cassie state as in Figs. 2(a) and (b). Also included are results calculated for the Wenzel state, and $\mu/\mu_g = 1$. The results are somewhat remarkable. We see that for relatively deep grooves, $e/\delta \geq 1$, $\beta^{x,y}$ profiles computed for different μ/μ_g , e/δ and even ϕ , practically converge into a single curve [33], which coincides with the numerical (but not semi-analytical) results reported before [15].

For shallow grooves ($e/\delta \leq 0.1$ for a longitudinal and $e/\delta \leq 0.25$ for a transverse case) the $\beta^{x,y}$ profiles depend only on the depth of the groove, and can be approximated by trapezoids with the central region of a constant slip given by Eq.(3), and linear edge regions where the local slip length is described by our asymptotic model.

B. Effective slip length

We finally turn to the effective slip lengths, which can be found by averaging the obtained numerical solution for longitudinal and transverse directions:

$$b_{\text{eff}}^{\parallel,\perp} = \frac{\langle u_{x,y} \rangle}{\langle \partial_z u_{x,y} \rangle} \Big|_{z=0}. \quad (10)$$

The calculations are made using the viscosity ratio of the Cassie and Wenzel states. For completeness we include the data for $\mu/\mu_g = 5$, which correspond to oil-impregnated textures. Fig. 6 shows longitudinal (a,b) and transverse (c,d) effective slip lengths as a function of solid fraction, $1 - \phi$, for shallow (a,c) and deep (b,d) grooves. The eigenvalues of the effective lengths of a striped surface with a *piecewise constant* local slip, $b_c^{x,y}$, have been calculated analytically [16]:

$$b_{\text{eff}}^{\parallel} \simeq \frac{L}{\pi} \frac{\ln \left[\sec \left(\frac{\pi\phi}{2} \right) \right]}{1 + \frac{L}{\pi b_c^x} \ln \left[\sec \left(\frac{\pi\phi}{2} \right) + \tan \left(\frac{\pi\phi}{2} \right) \right]}, \quad (11)$$

$$b_{\text{eff}}^{\perp} \simeq \frac{L}{2\pi} \frac{\ln \left[\sec \left(\frac{\pi\phi}{2} \right) \right]}{1 + \frac{L}{2\pi b_c^y} \ln \left[\sec \left(\frac{\pi\phi}{2} \right) + \tan \left(\frac{\pi\phi}{2} \right) \right]}.$$

Let us now try to define *apparent* constant local slip lengths at the gas sectors. Eq.(9) suggests the following definition

$$b_c^{x,y} = \delta \frac{\mu}{\mu_g} \beta_c^{x,y}, \quad (12)$$

where dimensionless slip lengths, $\beta_c^{x,y}$, depend only on the aspect ratio of the texture, e/δ . We fitted our theoretical results for $\mu/\mu_g = 5$ to Eq.(11) taking $\beta_c^{x,y}$ as a fitting parameter. The obtained values are surprisingly well described by simple functions

$$\beta_c^x \simeq \frac{\text{erf}(q_x e/\delta)}{q_x}, \quad \beta_c^y \simeq \frac{\text{erf}(q_y e/\delta)}{4q_y}, \quad (13)$$

with $q_x \simeq 3.1$ $q_y \simeq 2.17$. These functions saturate to $\beta_c^x \simeq 0.32$ and $\beta_c^y \simeq 0.12$ already at $e/\delta \geq 1$, by imposing constraints on the attainable $b_c^{x,y}$ (see Fig. 5).

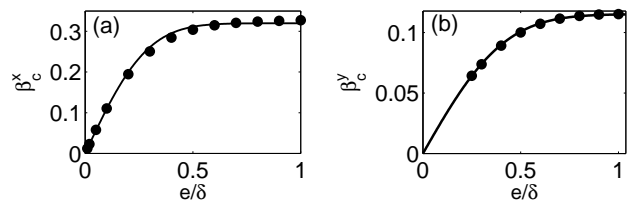


FIG. 5: Apparent local slip as a function of the depth of the groove for longitudinal (a) and transverse (b) directions. Symbols show the values obtained using Eqs.(11), solid curves show predictions of Eqs.(13).

Assuming $\beta_c^{x,y}$ found for $\mu/\mu_g = 5$ are universal, we can then use Eq.(11) to calculate the effective slip lengths for $\mu/\mu_g = 1$ and 50. The results are included in Fig.6. A general conclusion is that the predictions of Eq.(11) with the local slip defined by Eq.(12) are in excellent agreement with exact theoretical results in the whole range of parameters, $0.1 \leq \phi \leq 0.9$ and $\mu/\mu_g \geq 1$, confirming the universality of $\beta_c^{x,y}$. Note that included in Fig.6 effective slip lengths for perfect-slip stripes [10, 12], practically coincide with our results for $\mu/\mu_g = 50$. We can then conclude that SH surfaces in the Cassie state provide the very general upper bound for effective slip of textured surfaces, valid for whatever large viscosity contrast (e.g. polymer melts [34]). Finally, we observe an excellent agreement of our results for $\mu/\mu_g = 1$ with earlier data even for the Wenzel state obtained by using a completely different approach [31].

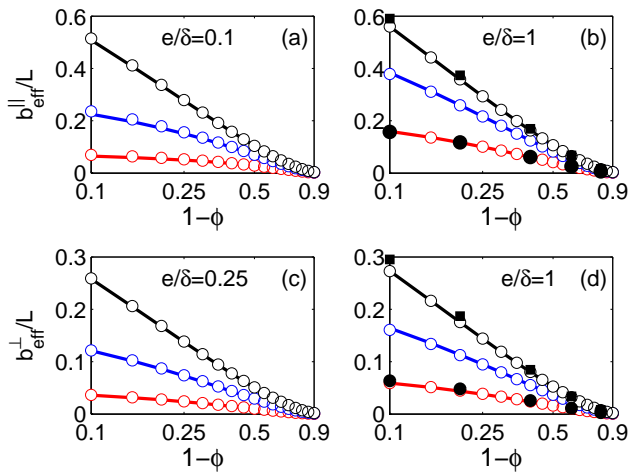


FIG. 6: Longitudinal (a,b) and transverse (c,d) effective slip lengths for textures with shallow (a,c) and deep (b,d) grooves. From top to bottom $\mu/\mu_g = 50, 5, 1$. Exact theoretical results are shown by circles, analytical results [Eq.(11)] with local slip given by Eq.(12) are plotted by solid curves. Filled squares show earlier data for perfect slip [10, 12], filled circles show earlier data for the Wenzel state [31].

Now, we recall that for pillars in the low ϕ limit, $\delta \simeq L$, the average local slip was shown to scale as [21]:

$$b_a^{x,y} \simeq L \frac{\mu}{\mu_g} \beta \tanh\left(\frac{e}{L\beta}\right) \quad (14)$$

with $\beta(\phi)$. For deep dilute pillars Eq.(14) transforms to $b_a^{x,y} \simeq L \frac{\mu}{\mu_g} \beta$ (cf. Eq.(12)), and for pillars with $\phi = 0.9$ we evaluate $\beta \simeq 0.2$ [21]. This value is close to the exact ones found here for deep rectangular grooves, $\beta_c^{x,y}$, so our theory provides a good sense of the possible local slip of 2D texture.

IV. CONCLUSION.

We have proposed an operator method, which allowed us the mapping of the flow in the gas subphase to a local slip boundary condition at the gas area of SH surfaces. The determined slip length is shown to be a unique function of the viscosity contrast and topography of the underlying texture. Our main results, Eqs.(9) and (12), can be thus viewed as a general ‘gas cushion’ model for textured surfaces, which transforms to the standard model, Eq.(3), in case of shallow textures. We have proven that besides Cassie surfaces our approach is valid for Wenzel textures, as well as rough surfaces impregnated by a ‘lubricant’ with lower viscosity.

We checked the validity of our approach by studying a flow past canonical rectangular grooves, but our strategy can be immediately applied for 1D textures with different cross-sections or extended to more complex 2D tex-

tures. These textures include various pillars, and holes and lamellae of a complex shape. Thus, our results may guide the design of textured surfaces with superlubricating potential in microfluidic devices, tribology, polymer science, and more. Another fruitful direction could be to apply our method to calculations of an electro-osmotic [35–37] and diffusio-osmotic [38] flow past textured surfaces.

Appendix A: Numerical solution in liquid

The non-local boundary condition given by Eq. (5) is easy to implement with the Fourier method. For simplicity we consider only the longitudinal flow here, the procedure for the transverse flow is similar. We present the flow over the superhydrophobic surface as a sum of the undisturbed flow and the correction due to the slip:

$$u_x(y, z) = u_0(z) + u_1(y, z),$$

where $u_0(z) = Gz$ is a simple shear flow and G is the undisturbed shear rate. The correction is sought in the form of a cosine series, since the solution is symmetric in y :

$$u_1(y, z) = c_0 + \sum_{m=1}^{\infty} c_m \cos(k_m y) \exp(-k_m z),$$

where $k_m = 2\pi m/L$.

Boundary conditions for the correction read:

$$\begin{aligned} \frac{\partial u_1}{\partial z} - \mathbf{P}^x[u_1] &= -G, & 0 < y < \delta/2, \\ u_1 &= 0, & \delta/2 < y < L/2. \end{aligned} \quad (A1)$$

(due to the symmetry of the problem, it is sufficient to consider only a half of the period). We take the same spatial grid that is used for the DtN matrix: $y_i = \delta\eta_i$ with N nodes over the groove

$$y_i = \delta(i-1)/2N, \quad i = 1 \dots N$$

and add M nodes at the boundary in contact with solid:

$$y_i = (L-\delta)(i-1)/[2(M-1)] + \delta/2, \quad i = N+1 \dots N+M.$$

We cut the series to $N_f = N + M$ terms and obtain the following linear system:

$$\begin{aligned} \sum_{m=1}^{N_f} D_{ik} c_m &= -G, & i &= 1 \dots N, \\ c_0 + \sum_{m=1}^{N_f} c_m \cos(k_m y_i) &= 0, & i &= N+1 \dots N_f, \end{aligned} \quad (A2)$$

$$D_{in} = k_n \cos(k_n y_i) - \sum_{j=1}^N P_{ij}^x \cos(k_n y_j).$$

Once the matrix P_{ij}^x is known, the linear system (A2) can be solved to find the correction, and the complete velocity field in liquid can be calculated. A similar procedure can be applied to the transverse flow (see [18] for reference).

Appendix B: Dirichlet-to-Neumann matrix for a rectangular groove

For rectangular geometries the Fourier method can be implemented to calculate the DtN matrices.

Longitudinal configuration. We introduce the non-dimensional variables in the gas domain, $\eta = y/\delta$ and $\zeta = z/\delta$. Following [14], we seek for the solution of the Laplace equation in gas in the form:

$$u_{gx}(\eta, \zeta) = \sum_{m=1}^{\infty} c_m \sinh[k_m^*(\zeta + d)] \cos(k_m^* \eta), \quad (\text{B1})$$

where $k_m^* = (2m - 1)\pi$, $d = e/\delta$. Each term in this series is a partial solution of the Laplace equation, which is symmetric in η and satisfies the no-slip boundary conditions at the side walls, $\eta = \pm 1/2$, and at the bottom wall of the groove, $\zeta = -d$, (see Fig. 1).

The velocity and its normal derivative at the liquid/gas interface are

$$\begin{aligned} \zeta = 0 : u_{gx} &= \sum_{m=1}^{\infty} c_m \sinh(k_m^* d) \cos(k_m^* \eta), \\ \frac{\partial u_{gx}}{\partial \zeta} &= \sum_{m=1}^{\infty} k_m^* c_m \cosh(k_m^* d) \cos(k_m^* \eta). \end{aligned} \quad (\text{B2})$$

The relation between them can be obtained from (B2):

$$\begin{aligned} \frac{\partial u_{gx}}{\partial \zeta} &= \sum_{m=1}^{\infty} (\Pi_{mn} u_n^*) \cos(k_m^* \eta), \\ u_n^* &= c_n \sinh(k_n^* d), \end{aligned}$$

$$\Pi_{ml} = k_m^* \coth(k_m^* e/\delta) \delta_{ml}, \quad m, l = 1.. \infty.$$

Here Π_{ml} is the representation of the DtN operator in the Fourier space.

The last step is to transform this operator into physical space, so that it can be applied as a boundary condition. To do so, we introduce a spatial grid $\eta_i = (i - 1)/(2N)$, $i = 1..N$ at the liquid/gas interface (due to the symmetry it is sufficient to consider only a half of the period) and cut the cosine series (B1) to N terms accordingly. Considering Eq. (B2) at each grid node we have:

$$u_{gx}(\eta_i, 0) = \sum_{m=1}^N F_{im} u_m^*,$$

and hence,

$$u_m^* = \sum_{i=1}^N F_{mi}^{-1} u_{gx}(\eta_i, 0),$$

where $F_{im} = \cos(k_m^* \eta_i)$ is the collocation matrix.

The normal derivative of the velocity (using dimensional variables y, z) reads:

$$\frac{\partial u_{gx}(\eta_i, 0)}{\partial z} = \sum_{j=1}^N P_{ij}^x u_{gx}(\eta_j, 0),$$

where

$$P_{ij}^x = \frac{1}{\delta} \left(F_{im} \Pi_{ml} F_{lj}^{-1} \right),$$

is the DtN matrix for the longitudinal flow.

Transverse configuration. We assume that the liquid/gas interface is flat, so that $u_{gz} = 0$ at $\zeta = 0$. The symmetry condition implies that u_{gy} is symmetric in η while u_{gz} is anti-symmetric. We represent the solution in gas in the following form [14]:

$$\begin{aligned} u_{gy}(\eta, \zeta) &= \sum_{n=1}^{\infty} \frac{\cos(k_n^* \eta)}{k_n^* \cosh(k_n^* d)} [A_n K'_n(\zeta) + B_n G'_n(\zeta)] \\ &+ \sum_{n=1}^{\infty} \cos(\beta_n \zeta) D_n H_n(\eta), \\ u_{gz}(\eta, \zeta) &= \sum_{n=1}^{\infty} \frac{\sin(k_n^* \eta)}{\cosh(k_n^* d)} [A_n K_n(\zeta) + B_n G_n(\zeta)] \\ &- \sum_{n=1}^{\infty} \sin(\beta_n \zeta) \frac{D_n}{\beta_n} H'_n(\eta), \end{aligned}$$

$$K_n = \sinh(k_n^* \zeta) - \zeta \exp[-k_n^*(\zeta + d)] \sinh(k_n^* d)/d,$$

$$G_n = k_n^* \zeta \sinh[k_n^*(\zeta + d)],$$

$$H_n = 2 \exp(-\beta_n/2) [\cosh(\beta_n \eta) - 2\eta \coth(\beta_n/2) \sinh(\beta_n \eta)].$$

where $k_n^* = (2n - 1)\pi$ and $\beta_n = n\pi d$; A_n , B_n and D_n are the unknown coefficients. The conditions of non-permeability at the side walls, $u_{gy} = 0$ at $\eta = \pm 1/2$, and at the bottom wall and at the interface, $u_{gz} = 0$ at $\zeta = 0, -d$, are satisfied automatically. The no-slip boundary conditions at the walls of the groove ($u_{gz} = 0$ at $\eta = \pm 1/2$ and $u_{gy} = 0$ at $\zeta = -d$) and the continuity condition at the interface ($u_{gy} = v^*$ at $\zeta = 0$) have to be satisfied by a proper choice of the coefficients A_n, B_n, D_n . To do so, we cut the series to N terms and introduce a grid covering the walls of the groove and the interface and containing $3N$ nodes (N at each wall/interface). Calculating the tangential velocity at each point of the groove, we obtain a system of $3N$ linear equations for a $3N$ -component vector $Z_k = \{A_1, \dots, A_N, B_1, \dots, B_N, D_1, \dots, D_N\}$. The right-hand sides of the equations are equal to zero at groove's walls (no-slip) and to liquid velocity at the interface, $u_{gy}(0, \eta_i) = v^*(\eta_i)$. The solution satisfying the no-slip boundary conditions and taking the prescribed values at the interface can be expressed in a matrix form:

$$Z_k = \sum_{j=0}^N M_{kj} v^*(\eta_j),$$

where $v^*(\eta_j)$ is a N -component vector of velocity at the interface grid points and M_{kj} is a $3N \times N$ matrix. Then the normal derivative at the interface can be expressed in the following way:

$$\frac{\partial v_g(\eta_j, 0)}{\partial \zeta} = \sum_{n=1}^N 2 \left[\frac{A_n}{d} \exp(-k_n^* d) \tanh(k_n^* d) + B_n k_n^* \right] \cos(k_n^* \eta_j) = Q_{ik} Z_k,$$

where Q_{ik} is $N \times 3N$ matrix.

Back in dimensional variables y, z , we obtain the following representation for the $N \times N$ DtN matrix :

$$P_{ij}^y = \delta^{-1} Q_{ik} M_{kj}.$$

Appendix C: Asymptotic solution near the edge of the grooves

Here we obtain a solution in the vicinity of the groove corner by using polar coordinates (r, θ) [30, 31], with the origin at $(y_c, z_c) = (-\delta/2, 0)$, so that $y = y_c + r\delta \cos \theta$, $z = r\delta \sin \theta$ (see Fig. 3(a)). Similar approach has been applied earlier for single-phase flows to describe singularities near sharp corners. For the flow over a surface with rectangular grooves, the shear stress has found to be singular, i.e., proportional to $r^{-1/3}$ for longitudinal and to $r^{-0.455}$ for transverse configurations [31]. The edge between different slipping flat interfaces has also been considered, with alternating no-slip and slip stripes [32, 39], trapezoidal and triangular profiles of the local slip $b(y)$ [30].

For the two-phase flow near the corner of a groove with flat interface, the liquid/solid, liquid/gas and gas/solid interfaces correspond to $\theta = 0$, $\theta = \pi$ and $\theta = 3\pi/2$ (if the wall of the groove is vertical). A general solution of the dimensionless Laplace equation is a power dependence on the distance r :

$$r \ll 1 : u_x = r^\lambda [a \sin(\lambda\theta) + g \cos(\lambda\theta)], \quad (C1)$$

$$u_{gx} = r^\lambda [c \sin(\lambda\theta) + h \cos(\lambda\theta)], \quad (C2)$$

where a, g, c and h are constants which may be found by matching (C1), (C2) with the flow at $r \sim 1$. However, the exponent λ can be obtained solely from the boundary conditions.

The no-slip boundary condition for liquid phase at $\theta = 0$, the no-slip boundary condition for gas phase at $\theta = 3\pi/2$ and the coupling conditions at the gas/liquid interface, Eq.(1), lead to a linear system on a, g, c, h which yields the following equation on λ :

$$\tan\left(\frac{3\lambda\pi}{2}\right) = \frac{(\mu - \mu_g) \tan(\lambda\pi)}{\mu + \mu_g \tan^2(\lambda\pi)}. \quad (C3)$$

Thus the exponent depends on the viscosity ratio μ/μ_g only. Previous analytical solutions, $\lambda = 2/3$, for a single-phase rectangular hydrophilic groove with $\mu/\mu_g = 1$ [31], and $\lambda_{\text{ideal}} = 1/2$ for a flat shear-free interface with $\mu/\mu_g = \infty$ [10, 39] satisfy the equation obtained. When the viscosity ratio is large, as for liquid/gas case, we construct an asymptotic solution of (C3) in terms of series in $\mu_g/\mu \ll 1$:

$$\lambda = \frac{1}{2} - \frac{\mu_g}{\mu\pi} + O\left(\frac{\mu_g^2}{\mu^2}\right). \quad (C4)$$

The asymptotic solution (C4) is close to that for alternating no-slip and perfect-slip stripes with $\lambda_{\text{ideal}} = 1/2$. The local slip length near the edge can be defined as

$$r \ll 1 : b_x(r) = \frac{u_x(r, \pi)}{\partial_\theta u_x(r, \pi)} \simeq 2 \frac{\mu}{\mu_g} r \delta.$$

Therefore, b_x is linear in the distance r from the corner at the liquid/gas interface. The slope of the dependence is large, of order of μ/μ_g .

For the flow transverse to the grooves, we represent the solution in liquid in terms of a streamfunction ψ which satisfies a biharmonic equation $\Delta^2 \psi = 0$. A general solution can be presented in the form [31]:

$$\psi(r, \theta) = r^\lambda [a \sin(\lambda\theta) + g \sin((\lambda - 2)\theta) + c \cos(\lambda\theta) + h \cos((\lambda - 2)\theta)]. \quad (C5)$$

The radial and the angular components of the liquid velocity are

$$u_r(r, \theta) = \frac{\partial_\theta \psi}{r}, \quad u_\theta(r, \theta) = -\partial_r \psi. \quad (C6)$$

Equations similar to (C5), (C6) can be also written for the gas streamfunction ψ_g and velocity components $u_{gr}, u_{g\theta}$. We apply the no-slip boundary conditions at $\theta = 0$ and $\theta = 3\pi/2$ and the continuity conditions at the gas/liquid interface, $\theta = \pi$, and, similar to (C3), we obtain the equation governing λ :

$$\frac{\tan(\lambda\pi)}{2(\lambda - 1)} = \frac{\mu}{\mu_g} \frac{2\lambda^2 - 4\lambda + 1 + \cos(\lambda\pi)}{4(1 - \lambda) \cos^2(\lambda\pi/2)}, \quad (C7)$$

For a shear-free interface, $\mu/\mu_g = \infty$, we have from (C7) $\lambda_{\text{ideal}} = 1/2$. Therefore, for large μ/μ_g we can again construct an asymptotic solution of (C7). The local slip length, to the first order in μ_g/μ , reads

$$r \ll 1 : b_y(r) = \frac{u_r(r, \pi)}{\partial_\theta u_r(r, \pi)} \simeq \frac{1}{2} \frac{\mu}{\mu_g} r \delta.$$

-
- [1] D. Quere, *Annu. Rev. Mater. Res.* **38**, 71 (2008).
- [2] L. Bocquet and J. L. Barrat, *Soft Matter* **3**, 685 (2007).
- [3] J. P. Rothstein, *Annu. Rev. Fluid Mech.* **42**, 89 (2010).
- [4] O. I. Vinogradova and A. L. Dubov, *Mendeleev Commun.* **19**, 229 (2012).
- [5] R. S. Voronov, D. V. Papavassiliou, and L. L. Lee, *Ind. Eng. Chem. Res.* **47**, 2455 (2008).
- [6] O. I. Vinogradova and A. V. Belyaev, *J. Phys.: Condens. Matter* **23**, 184104 (2011).
- [7] K. Kamrin, M. Z. Bazant, and H. A. Stone, *J. Fluid Mech.* **658**, 409 (2010).
- [8] H. A. Stone, A. D. Stroock, and A. Ajdari, *Annual Review of Fluid Mechanics* **36**, 381 (2004).
- [9] M. Z. Bazant and O. I. Vinogradova, *J. Fluid Mech.* **613**, 125 (2008).
- [10] J. R. Philip, *J. Appl. Math. Phys.* **23**, 353 (1972).
- [11] N. V. Priezjev, A. A. Darhuber, and S. M. Troian, *Phys. Rev. E* **71**, 041608 (2005).
- [12] E. Lauga and H. A. Stone, *J. Fluid Mech.* **489**, 55 (2003).
- [13] D. Maynes, K. Jeffs, B. Woolford, and B. W. Webb, *Phys. Fluids* **19**, 093603 (2007).
- [14] C. Ng, H. Chu, and C. Wang, *Phys. Fluids* **22**, 102002 (2010).
- [15] C. Schönecker, T. Baier, and S. Hardt, *J. Fluid Mech.* **740**, 168 (2014).
- [16] A. V. Belyaev and O. I. Vinogradova, *J. Fluid Mech.* **652**, 489 (2010).
- [17] O. I. Vinogradova, *Langmuir* **11**, 2213 (1995).
- [18] T. V. Nizkaya, E. S. Asmolov, and O. I. Vinogradova, *Soft Matter* **9**, 11671 (2013).
- [19] M. Sbragaglia and A. Prosperetti, *Phys. Fluids* **19**, 043603 (2007).
- [20] J. Hyväluoma and J. Harting, *Phys. Rev. Lett.* **100**, 246001 (2008).
- [21] C. Ybert, C. Barentin, C. Cottin-Bizonne, P. Joseph, and L. Bocquet, *Phys. Fluids* **19**, 123601 (2007).
- [22] E. Karatay, A. S. Haase, C. W. Visser, C. Sun, D. Lohse, P. A. Tsai, and R. G. H. Lammertink, *PNAS* **110**, 8422 (2013).
- [23] O. I. Vinogradova and G. E. Yakubov, *Langmuir* **19**, 1227 (2003).
- [24] C. Cottin-Bizonne, B. Cross, A. Steinberger, and E. Charlaix, *Phys. Rev. Lett.* **94**, 056102 (2005).
- [25] O. I. Vinogradova, K. Koynov, A. Best, and F. Feuillebois, *Phys. Rev. Lett.* **102**, 118302 (2009).
- [26] L. Joly, C. Ybert, and L. Bocquet, *Phys. Rev. Lett.* **96**, 046101 (2006).
- [27] D. Seo and W. A. Ducker, *Phys. Rev. Lett.* **111**, 174502 (2013).
- [28] A. Quarteroni and A. Valli, *Domain Decomposition Methods for Partial Differential Equations* (Oxford Science Publications, 1999).
- [29] C. Pozrikidis, *Boundary Integral and Singularity Methods for Linearised Viscous Flow* (Cambridge University Press, 1992).
- [30] J. Zhou, E. S. Asmolov, F. Schmid, and O. I. Vinogradova, *J. Chem. Phys.* **139**, 174708 (2013).
- [31] C. Y. Wang, *Phys. Fluids* **15**, 1114 (2003).
- [32] E. S. Asmolov, J. Zhou, F. Schmid, and O. I. Vinogradova, *Phys. Rev. E* **88**, 023004 (2013).
- [33] We remark that this curve can be very well fitted by a symmetric fourth-order polynomial with slopes defined by Eq.(8).
- [34] P. G. de Gennes, *C. R. Acad. Sci. Paris* **288 B**, 219 (1979).
- [35] A. V. Belyaev and O. I. Vinogradova, *Phys. Rev. Lett.* **107**, 098301 (2011).
- [36] T. M. Squires, *Phys. Fluids* **20**, 092105 (2008).
- [37] S. S. Bahga, O. I. Vinogradova, and M. Z. Bazant, *J. Fluid Mech.* **644**, 245 (2010).
- [38] D. M. Huang, C. Cottin-Bizzzone, C. Ybert, and L. Bocquet, *Phys. Rev. Lett.* **20**, 092105 (2008).
- [39] E. S. Asmolov and O. I. Vinogradova, *J. Fluid Mech.* **706**, 108 (2012).

